Springer

KSME

Journal of Mechanical Science and Technology 29 (9) (2015) 3919~3931
www.springerlink.com/content/1738-494x(Print)/1976-3824(Online)
DOI 10.1007/s12206-015-0838-y

Intelligent humanoid mobile robot with embedded control and stereo visual feedback †

Shiuh-Jer Huang*, Sheng Liu and Chun-His Wu

Department of Mechanical Engineering, National Taiwan University of Science and Technology, Taipei, 106, Taiwan

(Manuscript Received December 19, 2013; Revised February 9, 2015; Accepted May 11, 2015)

Abstract

Generally, an intelligent humanoid robot system should have dual arms, mobile ability and stereo vision for establishing the interactive capability in unknown environment. Stereo vision system detects unknown objects or obstacles from their visual range and estimates 3D coordinates in a working environment. Dual arms and mobile platform are employed to approach the detected object and execute interaction based on visual servo information. Here a wheel-based 10 DOF dual arms mobile robot with FPGA hardware control structure and a Digital signal processor (DSP) based CMOS stereo vision system was designed and built to construct an distributed embedded low cost visual guided intelligent robotic system. The intelligent fuzzy sliding mode control strategy was employed to design the robot arm and platform motion control system. The experimental results show that the proposed stereo vision algorithm has good recognition ability and accuracy. Each joint angular tracking error of humanoid robot can keep within 0.05° by using distributed FSMC controller.

Keywords: Mobile robot; Stereo vision; Fuzzy sliding model control; Embedded system

1. Introduction

Robotic systems have been widely applied in various industrial operations. Further researches are focused on precise mobility, interaction capability and multi-sensor fusion to increase robotic intelligent functions for future humanized dexterous applications. Hence, information technology, artificial intelligence and robotic technology are integrated together to develop an intelligent humanoid robot. Currently, infrared rays, lasers and ultrasonic sensors are used in mobile robot for obstacle avoidance. However, they cannot provide enough information for establishing robotic adaptability to environmental change and interactive motion. Many human daily actions are guided by the vision information of two eyes. Hence, the real-time machine vision is an important tool for intelligent mobile robot to work in interactive random environment. How to integrate the machine vision feedback information with robotic intelligent control strategy becomes a challenging research topic. The controller is expected to drive robotic arms for grasping static objects or tracking moving objects based on real-time vision servo scheme. The single camera visual feedback signal was first proposed by Shirai and Inoue [1] to correct the robot moving position. It can only provide 2D surface data without object depth information.

Stereo vision system was proposed by employing two cameras to take a pair of images for deriving the depth information from 2D plane images. Specific computation algorithms were proposed to simulate the parallax computation process of human brain. The object depth information can be estimated from the Sum of square difference (SSD) calculation of right-left cameras images [2]. Its applications will be greatly expected. However, the image processing operations of stereo vision need huge data handling, computing and large memory. Usually, they are constructed on PC based structure or parallel multi-CPU combination [3]. This hardware structure is not easy to implement on compact movable systems, i.e., mobile robot due to the volume and energy consumption factors. Fortunately, the operation speed and capacity of DSP and FPGA have been tremendously increasing in this decade due to the development of semi-conductors and digital circuit design technology. It is good enough for developing a stereo vision system of a movable stand-alone platform. TMS320C54x DSP is first employed to implement a single CCD camera image extraction system with 1.5 sec cycle time for 1M image pixels [4]. Bensrhair et al. [5] designed a simple stereo vision system with two CCD cameras by using three sets of TMS320C31 DSP to estimate the image depth information.

The vision servo robotic control system was first proposed by Hill and Park [6] for noncontact measuring purpose. Hutchinson et al. [7] established the overall literature review of visual servo robotic manipulators and classified them into

*Corresponding author. Tel.: +886 2 27376449, Fax.: +886 2 27376460
E-mail address: sjhuang@mail.ntust.edu.tw
† Recommended by Senior Editor Jong Hyeon Park
© KSME & Springer 2015

position-based and image-based two categories correlated to the error signal definition. Stereo vision was used to scan the robot environmental scene and construct the stereo geometric model or 2D plane map for mobile robot navigation and obstacle avoidance applications [8]. Kuo et al. [9] developed an image servo robotic control system for surgical application. Bonarini et al. [10] used an omnidirectional vision sensor for mobile robot motion control. Yang and Tayebi [11] developed a trajectory tracking controller for a B21R wheel mobile robot with a single vision camera and sonar sensors.

Hand-eye harmonizing capability is an important human advanced biological action. It should be a key function of a visual servo humanoid robotic system. Currently, how to develop a robotic control system with hand-eye coordination ability is a main research objective. Bais and Sablatnig [12] employed a visual system to detect color mark for omnidirectional mobile soccer robot positioning. Sabe et al. [13] integrated a stereo vision system with a humanoid robot for obstacle avoidance and path planning. These object extracting and locating strategies based on object image shifting due to relative motion and specific color characteristics have implementation difficulty and limitation for use on a mobile robot platform. Chen and Xu [14] installed one pair of image sensors on a mobile robot to build a passing 3D map based on stereo disparity. Elfes [15] used a disparity map for mobile robot perception and navigation. Wang et al. [16] employed right-left parallax images to dismember image and extract objects from a full image. It can be concluded that object depth information can be derived from disparity maps without specific object color or shape constraints. However, the accuracy of depth and 3D coordinates calculation, and implementation problem on mobile robot was not adequately discussed in previous researches. The stereo vision object detection strategy from an unknown environment and the integration of stereo vision system with mobile humanoid robot are still hot developing topics.

Here, a DSP processor is employed to construct a stereo vision system with two CMOS color image sensors and an FPGA chip is used to establish an intelligent control system for a dual arms mobile humanoid robot. The stereo vision system extracts the interactive target position and then sends it to the FPGA robotic servo controller as the motion command through the UART communication interface. Since the accurate dynamic model for a multi-axis humanoid robot is difficult to establish and the computation burden is overload for an embedded control chip due to the complicate nonlinear and coupling dynamics, the model-free intelligent control scheme is adopted in the robotic motion control field [17]. Generally, the design of a traditional fuzzy controller needs a time consuming trial-and-error process to establish suitable fuzzy rule bank for achieving the specified control performance. Here, 1D adaptive fuzzy sliding mode control strategy [18] is adopted and further modified to design each joint individual controller for a new built dual arms mobile humanoid robot. A novel gain scheduling algorithm is introduced to modify this-

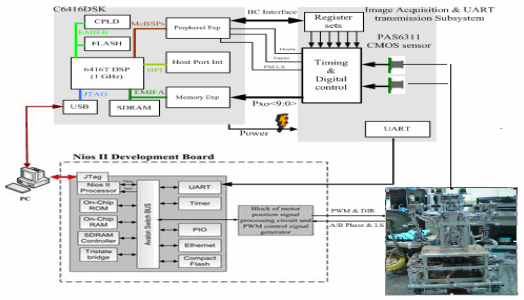

Fig. 1. Visual guided dual arms control system structure.

control algorithm for improving the overall control performance. It can on-line adjust the fuzzy control parameters in response to system transient and steady state responses requirement. This approach has light computation burden and is easy to implement on this embedded humanoid mobile robot for visual guided motion control purposes.

2. System structure and kinematics

The overall hardware structure of this visual servo dual arms humanoid mobile robot system is shown in Fig. 1. It can be divided into 10 DOF dual arms mechanism: a TMS320C 6416 DSP based stereo vision, a pair of CMOS image sensors and a Lab. made daughter card; an FPGA based dual arms mobile robot motion controller with a Atera Nios II embedded SOPC development kit; and four wheels moving platform four parts. The UART communication interface is designed to send the extracted object position and image pattern characteristics information from stereo vision system to SOPC robotic motion controller. Two PAS6311 CMOS color image sensors are selected to construct the stereo vision system, which is located on a pitch motion frame of robot for increasing the vision system viewing range. Each arm of this humanoid robot has five rotational degrees of freedom and one gripper. The Nios II development board is adopted to construct individual distributed motion controller for each joint of this robotic system. A PC is employed to install TI code composer studio of DSP developing software, Quartus II 6.1 and Nios II application software for developing the overall system control software.

The daughter card is designed to extract images from CMOS sensors and work as the UART communication interface. It includes DSK and CMOS I/O connection ports; RS232 interface conversion IC HIN232, voltage conversion IC Lm317 and Lm7805 and one oscillator for CMOS sensors external input timer. One port of DSP is specified as UART (RS232) communication port for sending the six bytes Cartesian coordinates information into FPGA robotic motion controller for visual servo purpose. The four wheels moving platform has two servo motors on right and left side, respectively, for motion control in 2D plane.

The dual arms humanoid robot and moving platform was designed and built in our Lab. The robotic manipulator link-

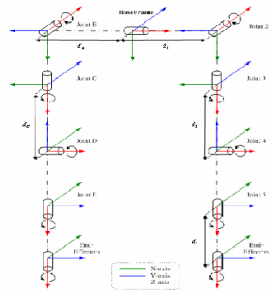

		α_i deg	a_i mm	d_i mm	θ_i (deg)
Right Arm	Joint A	-90	0	-200	θ_A
	Joint B	90	0	0	θ_B+90
	Joint C	-90	0	170	θ_C-90
	Joint D	90	0	0	θ_D
	Joint E	0	0	175	θ_E
Left Arm	Joint 1	-90	0	200	θ_1
	Joint 2	90	0	0	θ_2+90
	Joint 3	-90	0	170	θ_3+90
	Joint 4	90	0	0	θ_4
	Joint 5	0	0	175	θ_5

Fig. 2. Dual arms linkage coordinates system and Denavit-Hartenberg link parameters.

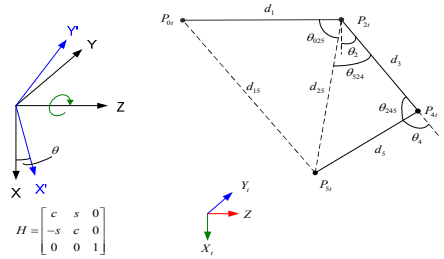

Fig. 3. Each angle geometric relationship for mode 1 joints 0, 2, 4 and 5 co-plane.

age connection plot and Denavit-Hartenberg link parameters are shown in Fig. 2. Generally, the end-effector working position or motion path in Cartesian space is converted into control variables in joint coordinates for controlling purpose by using the inverse kinematics and Denavit-Hartenberg transformation matrix. Although some efficient analysis methods have been proposed [19, 20], they are time consuming and complicated mathematical operations. Based on the robot link parameters, and forward kinematics calculation, the Denavit-Hartenberg transformation matrix can be derived and described by using the robotic D-H parameters a_i and θ_i. Since this stereo vision can only provide 3D Cartesian space coordinates without orientation information, the inverse kinematics solution for this 5 DOF arm has redundant DOF. We can specify two modes with joints 0, 2, 4 and 5 co-planarity or with joints 2, 4 and 5 on a plane. The selection of both modes depends on user and object location. Then the joint angle θ_i corresponding to the visual extracted object Cartesian coordinates $(p_{5t,}, p_{5t,y}, p_{5t,z})$ of mode 1, as Fig. 3, can be solved in FPGA controller by comparing the D-H matrix components and some trigonometric functions operations. Then, each joint angle can be calculated based on following steps.

$$\text{Step 1: } \theta_{025} = COS^{-1}\left(\frac{d_1^2 + {d_{25}}^2 - {d_{15}}^2}{2d_1 d_{25}}\right),$$

$$\theta_{524} = COS^{-1}\left(\frac{d_3^2 + {d_{25}}^2 - {d_5}^2}{2d_3 d_{25}}\right),$$

$$\theta_{245} = COS^{-1}\left(\frac{d_3^2 + {d_5}^2 - {d_{25}}^2}{2d_3 d_5}\right)$$

$$\text{Step 2: } \theta_1 = A\tan 2(p_{5x}, p_{5y})$$

$$\text{Step 3: } \theta_2 = \begin{cases} -(\theta_{025} + \theta_{524} - \pi/2) \\ -(\theta_{025} + \theta_{524} + \pi/2) \end{cases}, \begin{matrix} if\ \theta_{025} + \theta_{524} > \pi \\ otherwise \end{matrix} \quad (1)$$

$$\text{Step 4: } \theta_3 = \pi/2, \quad \theta_5 = -\pi/2$$

$$\text{Step 5: } \theta_4 = \pi - \theta_{245}.$$

For the multi-input and multi-output system, the motion trajectory of each joint corresponding to the end-effector Point to point (PTP) motion in Cartesian space needs be planned to move and stop at the same time for the simultaneous motion purpose. The trapezoid speed curve with a constant acceleration and deceleration time T_a, a constant acceleration value a_m and the total motion time T, is the most popular trajectory planning for the PTP motion. There relationships are

$$a_m T_a = v_m \quad \text{and} \quad T = \frac{X}{v_m} + T_a. \quad (2)$$

The axis with largest angular moving range is chosen to calculate the total motion time T based on the specified maximum acceleration, a_m, and maximum velocity, v_m. Then the acceleration time and the maximum velocity of the other axes can be derived based on these moving angles, total motion time and the maximum acceleration information.

$$T_{ai} = \frac{T}{2} - \sqrt{\frac{T^2}{4} - \frac{X_i}{a_m}} \quad \text{and} \quad v_m = a_m T_{ai}. \quad (3)$$

3. Image extraction system design

To integrate the DSK developing board and CMOS image sensors into a stereo vision system, the accompanying communication interface, image extracting daughter card, image pre-processing and appropriate time sequence control software need to be designed and built. They will be briefly explained in following sections. I2C communication interface was designed as bi-direction sequential data bus for master/slave transmission between two ICs with SCLK and SDA two lines. SCLK is the timing clock signal line come from master IC for synchronizing the time sequence of master and slave components. SDA is the data transfer line in response to the SCLK timing clock signal for executing the sequential data transfer. Here I2C is chosen as the data transfer interface between CMOS image sensors and DSK board. SDA and SCLK are directly connected to two GPIO pins on C6416DSK board. Appropriate control programs are designed to regulate the high-low change in GPIO pins for monitoring data transfer based on both lines rising and falling time sequence specifications. The I2C data bus format is 8 bits size without data number limitation. The main controller sends out an echo signal (ACK) following each transfer data byte. Then the data emitter releases the data line SDA and changes it to high level for receiver to send out ACK signal simultaneously. The corre-

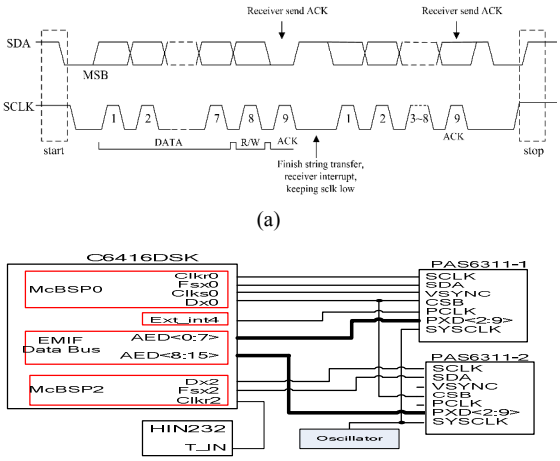

Fig. 4. (a) I2C data bus timing control sequence; (b) simplified daughter circuit board.

sponding SDA and SCLK timing control sequences for this I2C data transfer are shown in Fig. 4(a). In addition, a control program needs to be designed to synchronize the timing clock of CMOS image sensors and C6416DSK board for accurately transferring CMOS acquired image raw data into DSK board inside SDRAM.

The selected PAS106BCB283 CMOS image sensor needs an external timing clock signal with 48MHz default frequency. This pixel output clock (PCLK) is obtained by connecting the quartz oscillator signal into I2C frequency divider register with specified frequency. To extract the image signals from two CMOS sensors for DSP stereo vision calculation, the PCLK signal is used to synchronize the pixels data output operation. Vertical synchronize (VSYNC) is specified as the synchronous signal for each image transfer beginning clock. Horizontal synchronize (HSYNC) is used for raw pixels data transfer synchronizing. The VSYNC signal is accompanied with PCLK signal and external interrupt controller to command the C6416DSK for executing synchronize memory data read/write through the EDMA transfer channels [21]. The simplified daughter circuit board data flow is shown in Fig. 4(b).

Since stereo vision is based on two CMOS images to calculate 3D position, the extracted images synchronize is very important. Hence an appropriate checking process should be designed into the control software or this daughter circuit. Here two COMS sensors synchronize are obtained by using CSB enable control signal to actuate both image sensors for writing raw data into I2C register simultaneously. To guarantee the synchronous transmission of raw data from two CMOS image sensors, data contents should be inspected after the end of first data receiving process. The feature of ineffective DARK pixels in data format with fixed location can be specified as the checking point. If both received image raw data formats are not matched, the CSB enable control signal is restarted and checked it again.

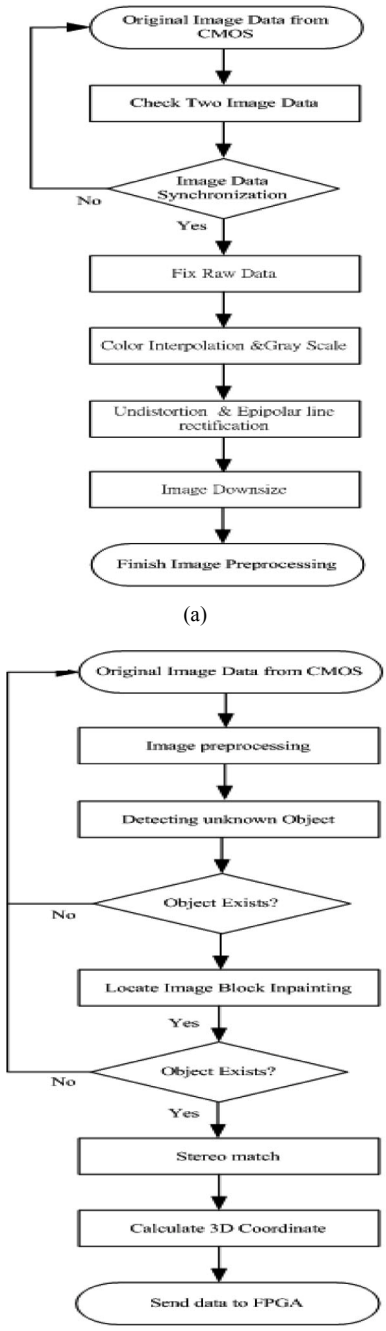

Fig. 5. (a) Image extracting and pre-processing flow chart; (b) stereo vision detecting and locating flow chart.

After the DSK board receives two sets of synchronous image raw data, following color interpolation, image gray scale calculation, image distortion calibration, epipolar line rectification and image downsize pre-processing operations are employed to recover the raw data into useful image information. The overall image extraction and pre-processing flow chart is shown in Fig. 5(a). The image preprocessing includes color interpolation to recover RGB colors, image gray operation, smoothing for eliminating noise and binary operations. YCbCr

color space is widely applied on digital image color space representation. The brightness gray signal is individually depicted as Y and the aberration signals are presented as Cb and Cr, where Cb is the color difference between blue and reference color (orange-blue axis), and Cr is the color difference between red and reference color (purple-red axis). The image pre-processing transforms the 8 bits image raw data of the pixel into 24 bits RBG color space data. To reduce the unnecessary calculation of DSP processor, the RGB image data is converted into 8 bits gray signal again by the following formula [22]:

$$\begin{bmatrix} Y \\ Cr \\ Cb \end{bmatrix} = \begin{bmatrix} 0.299 & 0.587 & 0.114 \\ -0.167 & -0.332 & 0.500 \\ 0.500 & -0.419 & -0.0813 \end{bmatrix} \begin{bmatrix} R \\ G \\ B \end{bmatrix}. \quad (4)$$

4. Object detecting and stereo matching in un- known environment

A stereo vision system is constructed to simulate human binocular vision feature for identifying the object in viewing space based on left-right disparity maps. How to distinguish the object from background in an image is an important technique for this object detection application. Different detecting schemes have been proposed for various objects and environments. If the shape or color of a specific object is pre-defined, their features can be used to simplify the object searching process [23]. However, their general purpose application is limited. Background subtraction scheme [24, 25] used a predefined environmental background model stored in database for comparing with current captured image. Subtracting the background image model from current extracted image information can obtain the coming or moving object. Its robustness and practical application for detecting moving object are limited to fixed background and vision system. It cannot be employed in mobile robot on board application. Here, a set of stereo vision object detecting and locating calculation algorithms are proposed for on-board mobile robot implementation. Horizontal and longitudinal projection schemes were employed to locate the relative positions of static and moving objects in a full picture. Since the projection algorithm is focused on one 2D image picture to locate the object area without any depth information, a pair of image pictures should be extracted simultaneously to execute the stereo matching and image depth calculation for constructing object 3D coordinates. The flow chart of stereo vision detecting and locating strategies is shown in Fig. 5(b).

4.1 Object detecting in unknown environment

The far and near judgment ability of humans is based on binocular parallax. The observation of both eyes for an object at different locations will construct an angle of parallax. The parallax characteristic depends on the depth between both eyes and object. The angle of parallax is inverse proportion to depth information. The disparity map related to right CMOS image can be established by minus each pixel gray value of left CMOS image jth raw from the corresponding right CMOS pixel with different column offset. The mathematical operation equation can be described as [26]:

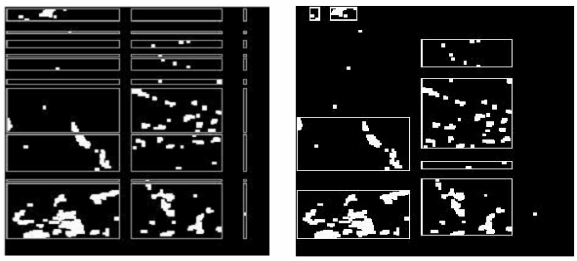

(a) (b)

Fig. 6. (a) 1st; (b) 2nd object projection searching results.

$$DSI_i^R(x,d) = I_R(x,i) - I_L(x+d,i) \text{ , when } 0 \le x+d < N. \quad (5)$$

Since the equivalent image width N depends on both CMOS installed position interval and detected object depth, the N value can be limited to an interesting relative depth $d_{\max}$ for significantly reducing computation burden. Then, the grand truth disparity map can be constructed by searching the minimum value of each pixel row from the disparity map and setting it as the disparity d of both images. It means that a pixel point of the left image is most similar to that of the right image with shifting distance d in horizontal direction. The value d is inversely proportional to the depth of the corresponding object. In addition, the point to block ($V \times H$) match scheme is employed to reduce the noise due to the parallelism defect of left-right images pair for improving the robustness. The operation equation can be written as:

$$DSI_i^R(x,d) = \underset{\substack{0 \le u < H/2 \\ 0 \le v < V/2}}{Min} [I_R(x,i) - I_L(x+d+u,i+v) \text{ , when } 0 \le x+d < N. \quad (6)$$

To improve the object block marking efficiency within a specified depth range and reduce the noise in grand truth disparity map, the binary, dilation and erosion morphological image processing schemes are introduced. In a binary picture, an object appears as white color and the background is depicted as black color, respectively. Based on horizontal and longitudinal projection operations, the relative position of object edges and background connection points can be marked in picture. For example, its mathematical operation equation in x direction can be represented as:

$$pjX_i = \sum_{y=0}^{height} frame(x_i, y). \quad (7)$$

If $pjX_{i-1} = 0$ and $pjX_i > 0$, means start point i of the object in x-axis.

If $pjX_i > 0$ and $pjX_{i+1} = 0$, means end point i of the object in x-axis.

It can be observed from Fig. 6 that certain image blocks with specific features were marked after this projection searching process. If the objects interval is too small or the object has surrounding noise, a couple of objects or surrounding noise will be marked together into a big block, as Fig. 6(a). Certain width or length threshold values should be selected to assist the object identification and scrappy noise elimination. In addition, second projection operation can be executed to distinguish too closing objects or eliminate object surrounding noise as Fig. 6(b). This projection operation can only be used to mark the possible object location in an image. Additional criteria should be set to extract the specified object position. Here, the size and height difference of marked objects in right and left images with projection operations are selected for comparison to accurately locate the specified object position.

4.2 Modification of the marked block location

Usually, the possible location of marked object block has certain offset or marked area uncertainty due to noise or incomplete depth disparity map. The following image processing schemes are adopted to correct the marked block location. First, the marked block area is enlarged to avoid the phenomenon that an object may not be included completely in a marked block due to object broken binary image. Then the most popular Gaussian smooth filtering scheme is employed to eliminate the noise data point from the gray scale image by using the convolution mathematical operation of Gaussian filter mask and target object image. Although the marked block of unknown object within depth map can provide the object rough skeleton coordinates, it is not good enough for extracting accurate object 3D location. Here, Sobel mask is introduced to enhance the high frequency part of the marked block image for detecting the target object edges. To enhance and isolate the target object image from the full image, the threshold automatic selection scheme [27] is employed for another binary operation. It can derive an appropriate binary threshold value based on statistics and classification concepts to establish maximum adjacent classes variance and minimum within class variance grouping. It can overcome the optic source and object moving variation factors. The Gaussian smooth filtering, Sobel edge detection and automatic binarization image processing results are shown in Figs. 7(a)-7(c), respectively. Finally, the projection algorithm can be used to extract and mark the target object block again for precise marking the target location. The differences between the marked target blocks of first and second projection operations are depicted in Figs. 7(d) and 7(e), respectively for comparison. It can be observed that the target object locating accuracy has been improved significantly.

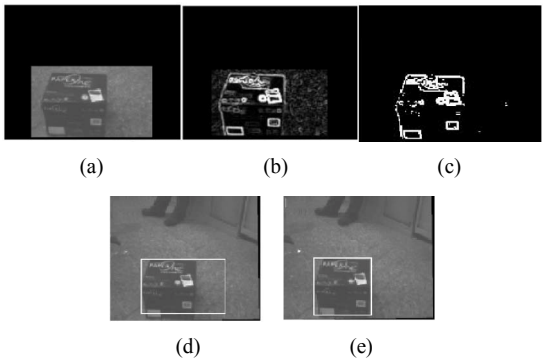

Fig. 7. (a) Gaussian smooth filtering; (b) Sobel edge detection; (c) automatic binarization image processing; (d) first; (e) second projection operations results of marked target blocks.

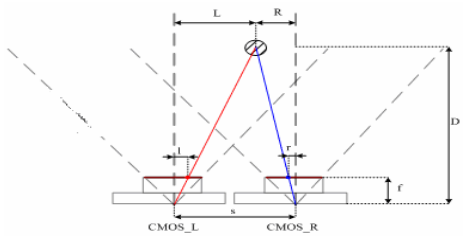

Fig. 8. Optical geometry relationship of stereo vision system.

4.3 Stereo vision structure and stereo matching operation

When we close one eye, all the object points in image projection line diffused from foci with different distances from the eye will be projected at the same point on the image plane. The depth difference between them cannot be estimated. Hence, another eye is required to extract the corresponding information for constructing stereo vision. The well accepted stereo vision system structure is constructed with two image sensors. The depth information can be calculated based on the optical geometrical relationship of both left-right image sensors, as Fig. 8. This setup can distinguish the depth information difference of those points located in an image projection line of one CMOS sensor.

Each COMS image sensor has its own focus and maximum viewing angle specification. For stereo vision detecting and measuring purposes, the object must be located within the overlapped zone of both CMOS image sensors visible ranges. This common visible zone depends on the COMS specifications, two sensors installation interval and the angle between both CMOS optical axes. Here two CMOS are horizontally installed with 12.7 cm interval to simulate human both eyes, and both optical axes are parallel to simplify the 3D coordinate calculation. It is located at the head part of a humanoid robot and integrated with this dual arms mobile humanoid robotic system for future intelligent application purposes. To derive accurate 3D coordinates based on this stereo vision system, both parallel optical axes need to be calibrated experimentally. The pixel space in image plane of this CMOS sensor is 3.6 μm x 3.6 μm found from specification. It can be

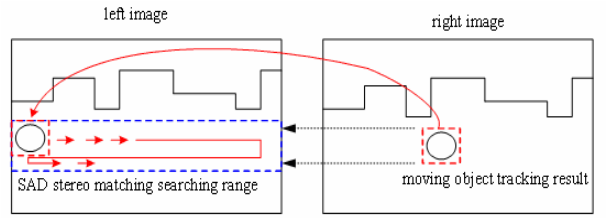

Fig. 9. Searching area definition by using SAD direct stereo matching.

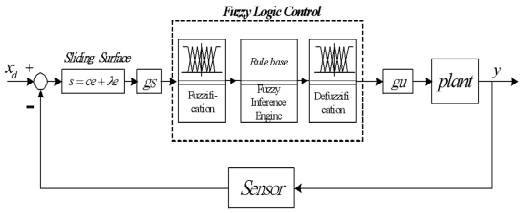

Fig. 10. Fuzzy sliding mode control block diagram.

used to calculate the CMOS focus based on the optical geometry relationship as Fig. 8. The calculation value is 2.74 mm.

Stereo matching is to locate a specified target point of an object on a pair of left-right images with a fixed position dislocation. It can be classified into active and passive types. It is the necessary procedure for 3D coordinates calculation. Active stereo matching is executed by finding the corresponding positions on both left-right images of a laser light spot pointed on object. Their dislocation value can be used for 3D coordinate calculation. The passive stereo matching methods are performed by using the characteristic point of left-right images, for example: direct matching, block gray scale comparison, edge, projection, etc. Here, direct matching scheme and Sum of absolutely difference (SAD) algorithm are adopted for stereo matching operation. SAD method needs a reference target pattern to search the minimum SAD value location within a specified area of extracted image for locating the object position. Its mathematical equation can be written as [24]:

$$SAD(x,y)=\sum_{i=0}^{(ref_H-1)}\sum_{j=0}^{(ref_W-1)}\left|frame(x+i,y+j)-ref(x,y)\right| \tag{8}$$

where SAD(x,y) is the SAD calculation value at point (x, y) inside the specified area, *frame* represents current image, *ref* depicts the moving object reference pattern, ref_H and ref_W are the height and width of reference pattern, respectively. Generally, they are defined as the precise moving object 2D dimension. Twice values of ref_H and ref_W are selected as the specified searching range of each operation cycle. The position with minimum SAD value is specified as the new location of this target object.

When the SAD scheme has marked an unknown moving target based on right hand side CMOS image, the reference moving target pattern is updated and used to search the matching object on left hand side image. Since two CMOS image sensors are horizontally installed with parallel optical axes, they will be expected to have a horizontal direction pixels shifting. Hence the searching area on the left hand side image is limited to about the same height as that of reference target object pattern in right image with two more pixel rows, as Fig. 9. The corresponding position of the minimum SAD value in the left hand side image is marked as the stereo matching point of this moving object.

4.4 Object depth estimation and 3D coordinate calculation

When the target object was marked and the stereo matching operation was completed, the object depth could be estimated for 3D coordinate calculation. The optical geometry relationship of this stereo vision system can be displayed as Fig. 7. Then the object depth D can be derived as

$$\frac{L}{l}=\frac{D}{f},\frac{R}{r}=\frac{D}{f} \tag{9}$$

$$s=L+R=(l\times\frac{D}{f})+(r\times\frac{D}{f})=(l+r)\times\frac{D}{f} \tag{10}$$

$$D=\frac{s\times f}{l+r}, \tag{11}$$

where f is the CMOS focus, s is the distance between both CMOS sensors. L and r are the lengths of targeted object with respect to left and right CMOS optical axes, respectively.

Then 3D coordinates of this moving object can be calculated based on the defined coordinate direction as Fig. 8.

5. Humanoid mobile robot motion control algorithm

Since the multi degrees of freedom robotic control system has nonlinear and complicated dynamics behavior, it is difficult to establish an appropriate dynamic model for the model based controller design, especially for the embedded controller. Here the sliding mode concept [28, 29] is combined with fuzzy control strategy to design a model-free Fuzzy sliding mode controller (FSMC) for robotic motion control. In addition, the fuzzy variables gains scheduling strategy is integrated into the model-free fuzzy sliding mode control scheme for improving the transient response and steady state error performance. The fuzzy sliding control scheme with fuzzy variables gain scheduling control block diagram is shown in Fig. 10. It is an enhanced and extended new development based on the original FSMC approach proposed by Huang and Lin [18] to achieve excellent dynamic performance.

5.1 FSMC robotic joint controller

A sliding surface on the phase plane is defined as

$$s(t)=(\frac{d}{dt}+\lambda)e_1=ae_2+be_1, \tag{12}$$

where $e_i = x_{id} - x_i$ are defined as the state control errors. This sliding variable, s, will be used as the input signal for establishing a fuzzy logic control system to approximate the specified perfect control law, u_{eq}. The perfect control law is defined as the calculated control law based on sliding mode controller algorithm and accurate system dynamic model. With this perfect control law, the closed loop control system has an asymptotical stability dynamic behavior.

$$\dot{s}(t) + \lambda s(t) = 0. \tag{13}$$

Since λ is a positive value, the sliding surface variable, s, will gradually converge to zero. Based on the definition of sliding surface variable, s, in Eq. (12), the system output error will converge to zero, too. In this study, a fuzzy system is employed to approximate the mapping between the sliding variable, s, and the control law, u, instead of model-based calculation. This control law may have certain difference with respect to the perfect control law u_{eq}, then the following equation can be derived [18].

$$\dot{s}(t) = -\lambda s(t) + b(X,t)[u_{eq}(t) - u(t)]. \tag{14}$$

Generally, $b(X)$ is a positive constant or a positive slow time-varying function for practical physical systems. By multiplying both sides of the above equation with s gives

$$s(t)\dot{s}(t) = s(t)\{-\lambda s(t) + b(X,t)[u_{eq}(t) - u(t)]\}. \tag{15}$$

Based on the Lyapunov theorem, the sliding surface reaching condition is $s \cdot \dot{s} < 0$. If a control input u can be chosen to satisfy this reaching condition, the control system will converge to the origin of the phase plane. It can also be found that $\dot{s}$ increases as u decreases and vice versa in Eq. (14). If $s > 0$, then the increasing of u will result in $s\dot{s}$ decreasing. When the condition is $s < 0$, $s\dot{s}$ will decrease with the decreasing of u. Based on this qualitative analysis, the control input u can be designed in an attempt to satisfy the inequality $s \cdot \dot{s} < 0$. The related theory about the convergence and stability of the adaptation process on the basis of the minimization of $s\dot{s}$ can be found in Ref. [30].

Here, a fuzzy logic control is employed to approximate the nonlinear function of equivalent control law, u_{eq}. The control voltage change for each sampling step is derived from fuzzy inference and defuzzification calculation instead of the equivalent control law derived from the nominal model at the sliding surface. It can eliminate the chattering phenomenon of a traditional sliding mode control. The controller design does not need a mathematical model and without constant gain limitation. The system control block diagram is shown in Fig. 10. The one-dimensional fuzzy rules, Fig. 11(b), are designed based on the sliding surface reaching condition, $s \cdot \dot{s} < 0$. The sliding surface variable, s, is employed as the one-dimensional fuzzy input variable.

Here, eleven fuzzy rules are employed in this control system to obtain appropriate dynamic response and control accuracy. The input membership functions are scaled into the range of -1 and +1 with equal span. Hence a scaling factor gs is employed to map the sliding surface variable, s, into this universe of discourse. A scaling factor gu is used to adjust the value of control voltage. Membership functions of fuzzy input and output variables, and the fuzzy rules of the FSMC are shown in Figs. 11(a) and 11(b), respectively. The divisions of this membership functions can be expanded or shrunk by changing the scaling parameter of membership functions. These mapping parameters are specified as gs, and gu for the sliding variable and control voltage, respectively. The parameter values a, b, gs and gu for each

Table 1. FSMC gain parameters.

	Joint 1	Joint 2	Joint 3	Joint 4	Joint 5
a	15	15	15	15	10
b	1	1	1	1	1
Gu	1733(3.6V)	1064(3.3V)	1064(3.3V)	1064(3.3V)	98.3(1.44V)
gs	2.5	3.0	3.0	1.5	1.0

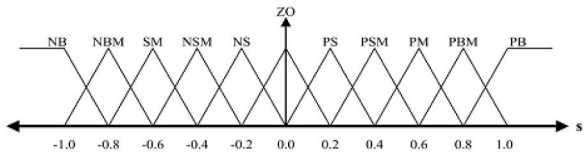

(a)

Sliding Surface	S									
	NB	NBM	NM	NSM	NS	ZO	PS	PSM	PM	PBM	PB
Control Rule	-1.0	-0.8	-0.6	-0.4	-0.2	0.0	0.05	0.1	0.2	0.4	0.6

(b)

Fig. 11. (a) Sliding variables fuzzy membership functions; (b) joints fuzzy control parameters and fuzzy control rules.

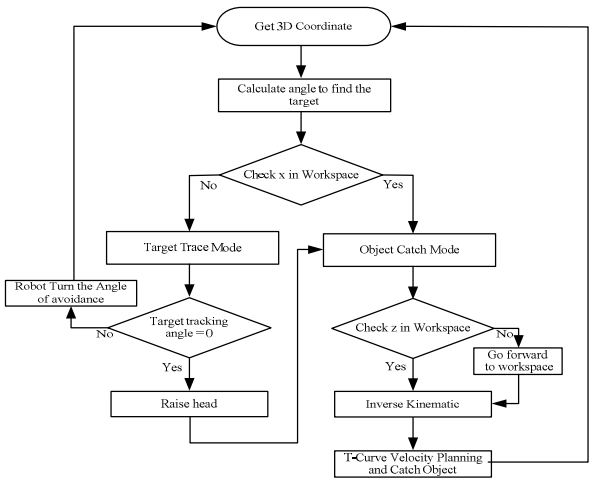

Fig. 12. Control flow chart of mobile robot to find an unknown object and catch it in unknown environment.

Table 2. Vertical block 3D coordinates estimation and error percentage.

Image coordinate R	(66, 58)~(88, 108)	Image coordinate L	(128, 58)~(150, 108)
3D coordinate (Estimate/actual)	X: 119.07/120(mm)	Y: -281.31/-290(mm)	Z: -53.12/-55(mm)
Error 3D coordinate (Estimate/rate)	X: 0.93(mm)/0.77(%)	Y: 8.69(mm)/3(%)	Z: 1.88(mm)/3.42(%)
Size (Estimate/actual)	Height: 104.19/95(mm)	Width: 46.99/42(mm)	Length: 72/60(mm)
Catch mode	Straight object		
Pixel resolution (mm/pixel)	2.0		

Table 3. Cubic box 3D dimension and coordinates estimation results.

Image coordinate R	(35, 63)~(95, 114)	Image coordinate L	(62, 63)~(122, 114)
3D coordinate (Estimate/actual)	X: 470.30/480(mm)	Y: -652.2344/-660.0(mm)	Z: 16.41953/18(mm)
Error 3D coordinate (Estimate/rate)	X: 9.7018(mm)/2.02(%)	Y: 7.7656(mm)/1.18(%)	Z: 1.5805(mm)/8.78(%)
Size (Estimate/actual)	Height: 243.95/240(mm)	Width: 286.17/310(mm)	Length: 202.0/230(mm)
Catch mode	Horizontal object		
Pixel resolution (mm/pixel)	5.1667		

Table 4. Multi-box object 3D dimension and coordinates estimation results.

Object 1			
Image coordinate R	(2, 52)~(61, 107)	Image coordinate L	(27, 52)~(86, 107)
3D coordinate (Estimate/actual)	X: 480.83/480(mm)	Y: -731.27/-770(mm)	Z: 195.06/210(mm)
Error 3D coordinate (Estimate/rate)	X: 0.83(mm)/0.17(%)	Y: 38.73(mm)/5.03(%)	Z: 14.936(mm)/7.11(%)
Size (Estimate/actual)	Height: 283.73/240(mm)	Width: 298.93/310(mm)	Length: 235.0/230(mm)
Object 2			
Image coordinate R	(82, 59)~(128, 113)	Image coordinate L	(108, 59)~(154, 113)
3D coordinate (Estimate/actual)	X: 485.458/490(mm)	Y: -683.42/-700(mm)	Z: -189.997/-178(mm)
Error 3D coordinate (Estimate/rate)	X: 4.542(mm)/0.93(%)	Y: 16.578(mm)/2.37(%)	Z: 11.997(mm)/6.74(%)
Size (Estimate/actual)	Height: 272.82/230(mm)	Width: 238.72/250(mm)	Length: 226.0/240(mm)
Pixel resolution (mm/pixel)	4.6296		

joint are listed on Table 1. This approach is a novel gain scheduling 1D fuzzy sliding mode control structure. The values of these parameters are not critical for this gain scheduling fuzzy sliding mode controller. They can be roughly determined by simple experimental tests.

5.2 Humanoid mobile robot control strategy

To achieve the intelligent functions of a humanoid mobile robot for working in an unknown environment, there should be an appropriate control strategy to integrate the platform mobility and stereo vision searching results for obstacle avoidance and object tracking or catching. For example, the control flow chart for a mobile robot to find an unknown object in an unknown environment and catch it is shown in Fig. 12. After the stereo vision extracting the target object 3D coordinates and size, a simple geometric operation can be used to find the platform rotation angle for tracking or avoiding the target. If there are obstacles between the robot and target, the mobile robot will bypass the obstacle with a planned path. The control program continuously checks the target object within the humanoid robot workspace or not with a specified cycle time for executing following robot hand catching mode or maintaining reaching/ avoiding mode selection.

6. Experimental results and discussion

To evaluate the dynamic performance of this visually guided humanoid mobile robotic system, and implementation limitation, the following experiments are planned and investigated. Both the software programs and hardware system structure are tested with practical application conditions. These experiments can be divided into stereo vision performances analysis, humanoid robot motion control accuracy evaluation and the intelligent interaction application of the visual guided humanoid mobile robot three parts.

6.1 Image processing operation time and unknown object detecting efficiency

The image processing software programs include raw data extracting, image preprocessing, disparity map, morphological

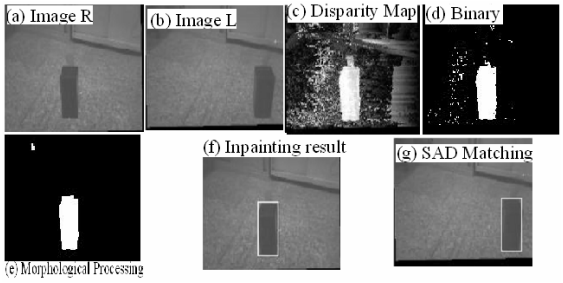

Fig. 13. A vertical block detecting and locating image processing results.

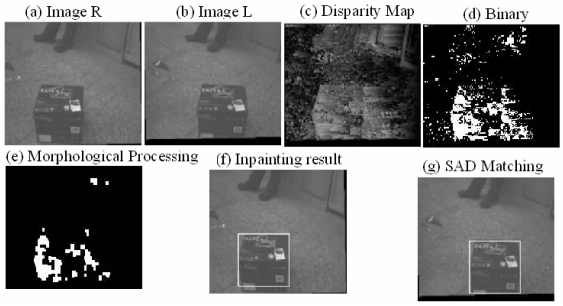

Fig. 14. A cubic box detecting and locating image processing results.

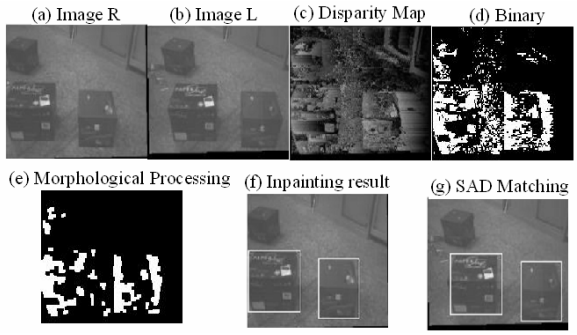

Fig. 15. Multi- cubic box detecting and locating image processing results.

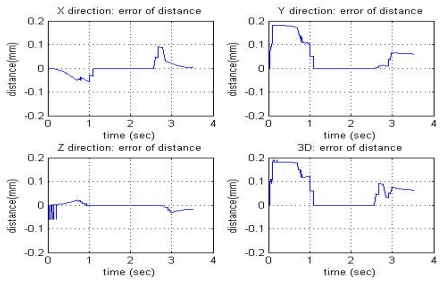

Fig. 16. The trajectory error curves of X, Y and Z coordinates and 3D contouring error.

processing, unknown object locating, stereo matching and 3D coordinates calculation. After ten times of experimental tests, their average executing times were 25.6 ms, 14.7 ms, 102.2 ms, 4.2 ms, 5.8 ms, 40.5 ms and 2.3 ms, respectively. Hence the DSP stereo vision image processing frequency was set as 2 Hz. A vertical block was randomly placed at a near distance inside this stereo vision viewing range. Its image processing results, 3D coordinates locating and dimension estimation results are shown in Fig. 13 and Table 2. It can be observed that the 3D coordinate error is less than 3.5%, the dimensional error is less than 6 pixels resolution. A cubic box is randomly placed at a far distance inside this stereo vision viewing range. Its image processing results, 3D coordinates locating and dimension estimation results are shown in Fig. 14 and Table 3. It can be observed that the 3D coordinate error is less than 2 % in height and width directions and 8.8% in depth direction. The dimensional error is less than 6 pixels resolution. For the third experiment, three cubic boxes are randomly placed in different distances from the stereo vision system. Two near object boxes are extracted by setting an interesting relative depth $d_{\max}$ to eliminate the far box during the targets blocking step. Its image processing results, 3D coordinates locating and dimension estimation results are shown in Fig. 15 and Table 4. The 3D coordinate error is less than 3.5%. The object boxes dimensions are roughly estimated, too.

6.2 FSMC robotic motion control accuracy and stereo vision integration accuracy investigation

Before executing the overall visual guided humanoid robotic motion control application, the robotic P-T-P set points control accuracy of both arms using fuzzy sliding mode controller are checked first. The end-effector of the right arm is specified to move from (345, 0, 200) mm to (-50, -212, 50) mm with a T-curve speed plan for each joint angle. The final state control error are (0.034, 0.061, -0.018) mm for right arm end-effector. The trajectory error curves of X, Y and Z coordinates and 3D contouring error are shown in Fig. 16. The maximum angular tacking error for each joint is less than 0.02°. The end-effector maximum 3D position tracking error is less than (0.091, 0.182, 0.032) mm. It is good enough and acceptable for the object grasping with dimension from 20 mm to 50 mm.

6.3 Embedded stereo vision and mobile humanoid robot integration applications

To evaluate the feasibility of visually guided humanoid mobile robot autonomous grasping an unknown object in varying environment, four experiments were executed in random environment for humanoid robotic end-effector to grasp or contact with specific target based on stereo vision command. The strike-rate depends on the end-effector motion control accuracy and the corresponding stereo vision 3D coordinates analysis accuracy.

Case (1): Detect and grasp a hand hold object within humanoid robot working space

The player randomly holds an object by hand and moves into the stereo vision viewing range and end-effector working space of this intelligent humanoid mobile robot. The proposed stereo vision is used to detect the proximal interesting object

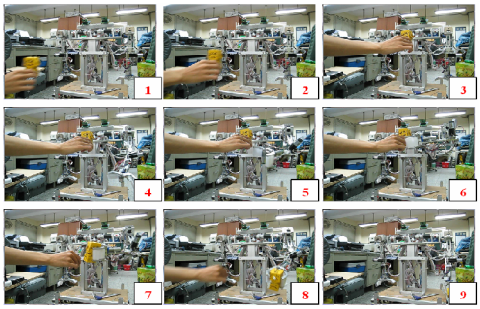

Fig. 17. Nine sequential operation pictures of humanoid robot detect object in player hand and grasp it with robotic left end-effector.

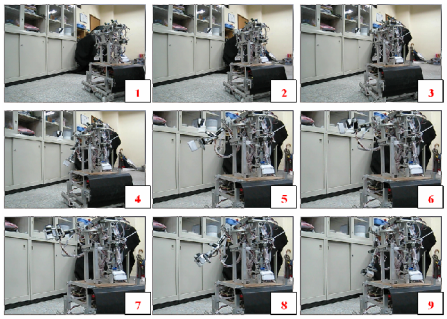

Fig. 18. Nine sequential operation pictures of humanoid robot detect object hanging in space and grasping it with robotic right end-effector.

and calculate the object 3D position. Then, the 3D coordinates information is sent to the mobile robot FPGA controller for judging following moving platform approaching or end-effector grasping operation modes selection. Since the target object has already been located within the robot working space, the mobile humanoid robot can proceed to the end-effector grasping operation directly based on 3D information and inverse kinematics without any platform motion. Nine sequential pictures are shown in Fig. 17 to demo its operation process and effectiveness. It can be concluded that the interesting target can be extracted from multiobjects environment by using relative depth setting and grasped with precise motion control algorithm.

Case (2): Detect and grasp an unknown object outside robot working space

An object is hanged in Cartesian space outside the robotic end-effector working space and there is no obstacle between object and robot. The stereo vision system is used to detect the proximal interesting object and calculate the object 3D location. Then, the 3D coordinates information is sent to mobile robot FPGA controller for use as a target position to guide humanoid mobile robot approaching an end-effector grasping space position with appropriate motion path planning. Hence, the humanoid can lift one hand to grasp the target object based on robot arm inverse kinematics and motion control scheme. Nine sequential pictures are shown in Fig. 18 to demo its operation process and effectiveness. It can be concluded that the unknown target can be extracted from 3D un-autonomous environment

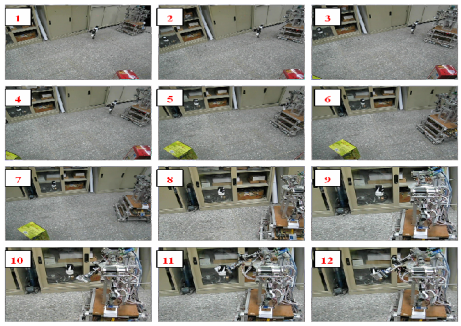

Fig. 19. Twelve sequential operation pictures of humanoid robot detecting object hanging in 3D space, and obstacle in floor, and robot bypass obstacle to grasp the target object.

and successfully grasped by robotic end-effector with precise robot arm and mobile platform motion control algorithm.

Case (3): Detect obstacle and unknown object outside working space for safe approaching and grasping

To evaluate this humanoid robot intelligent capability for working in random environment with obstacle, a target object is hanged at a far distance in Cartesian space and two obstacles are placed on floor between robot platform and object pick up position. The proposed stereo vision system is employed to detect multi objects and locate their 3D dimensions and locations. The detected objects on the floor are classified as obstacles and the other object is specified as target object. Then, an appropriate mobile robot motion path is planned on-line between target position and mobile robot current location based on obstacles by pass avoidance scheme. Stereo vision system is real-time tracking the obstacle 3D position for making sure of the robot motion path free of obstacle collision. The obstacle avoidance motion path is planned on-line to bypass each obstacle one by one. After humanoid robot passing obstacles, it is planned to approach the target object till a specified position, where robot end-effector can reach and grasp the object. Then, the humanoid can lift one hand to grasp the target object based on robot arm inverse kinematics and motion control scheme. Twelve sequential pictures are shown in Fig. 19 to demo its operation process and effectiveness. It can be concluded that the unknown target and obstacle can be extracted from 3D un-autonomous environment and the mobile robot motion control strategy can successfully avoid the floor obstacles to approach and grasp the target object by robotic end-effector with precise robot arm and mobile platform motion control algorithm.

Case (4): Detect interesting object and interaction with it in unknown environment

To evaluate this humanoid robot interaction function with interesting target in random environment with obstacle, a toy pug is set on a chair at a far distance outside the robot working space, and one cubic box obstacle is placed on the floor between robot platform and target object. The scenario is planned as the mobile humanoid robot needs to bypass the

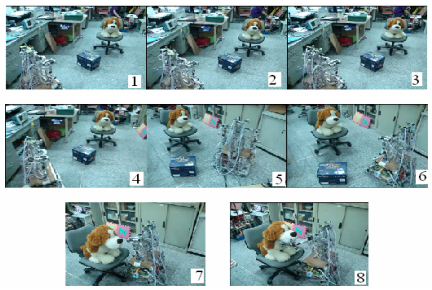

Fig. 20. Eight sequential operation pictures of humanoid robot detect toll pug and light touch its chin with left end-effector.

obstacle and approach the toy pug and use the left hand end-effector to lightly touch the toy pug's chin. The proposed stereo vision system is employed to detect toy pug and obstacle 3D dimensions and locations. Then, an appropriate mobile robot motion path is planned between toy pug position and mobile robot current location based on obstacle by pass avoidance scheme. After the humanoid robot approaches a specified position, the head part of the toy pug is within the working space of the mobile robot end-effector. Then, the humanoid can lift one hand with end-effect to touch the chin of the toy pug lightly based on robot arm inverse kinematics and motion control scheme. Eight sequential operation pictures are shown in Fig. 20 to demo this interaction operation.

7. Conclusion

An industrial DSP developing kit was integrated with two CMOS image color sensors to construct a cheap stereo vision system with 2 frame/sec capability for mobile robot application purpose. The intelligent fuzzy sliding mode control scheme was proposed for designing the FPGA based dual arm humanoid mobile robot motion control system. This 3D visual guided robotic system can detect static/moving objects and send the location information through UART interface to humanoid mobile robot FPGA control structure for driving robotic arms to grasp it or bypass the obstacle. That constitutes the basic intelligent humanoid mobile robot functions. Experimental results show that this low cost novel system can execute certain unknown object detection and 3D coordinates estimation in a random environment and the mobile robot can use these coordinates information for executing obstacle avoidance and target object grasping or interaction. These good features are useful for future humanoid mobile robot interactive implementation in unknown environment. The system robustness function, response speed and control accuracy are future research objectives.

Acknowledgment

This work was supported by the National Science Council Foundation of Taiwan under the Grant No. NSC- 95-2221-E-011-156 -MY3.

References

[1] Y. Shirai and H. Inoue, Guiding a robot by visual feedback assembling tasks, *Pattern Recognition,* Pergamon Press, 5 (1973) 99-108.

[2] T. Kanade, A. Yoshida, K. Oda, H. Kano and M. Tanaka, A stereo machine for video-rate dense depth mapping and its new applications, *Proceedings of the 15th Computer Vision and Pattern Recognition Conference (ICVPR'96)*, June (1996) 196-202.

[3] A. Bensrhair, N. Chafiqui and P. Michel, Implementation of a 3D vision system on DSP4 TMS320C31, *Real-Time Imaging*, 6 (2000) 213-221.

[4] K. Illgner, H. G. Gruber, P. Gelabert, J. Liang, Y. Yoo, W. Rabadi and R. Talluri, Programable DSP platform for digital still cameras, *Proceedings of IEEE International Conference on Acoustics, Speech, Signal Processing* ICASSP'99, 4, Phoenix, Arizona, USA, March (1999) 2235-2238.

[5] L. Lei, X. Zhou and M. Pan, Automated vision inspection system for the size measurement of workpieces, *Proceedings of the IEEE Instrumentation and Measurement Technology Conference,* IMTC, Ontario, Canada, 2, May (2005) 872-877.

[6] J. Hill and W. T. Park, Real time control of a robot with a mobile camera, *Proceedings of the 9th ISIR*, Washington, D.C., USA (1979) 222-246.

[7] A. C. Hutchison, G. D. Hager and P. J. Corke, A tutorial on visual servo control, *IEEE Transactions on Robotics and Automation*, 12 (5) (1996) 651-668.

[8] T. Kanade, A. Yoshida, K. Oda, H. Kano and M. Tanaka, A stereo machine for video-rate dense depth mapping and its new applications, *Proceedings of the 15th Computer Vision and Pattern Recognition Conference (ICVPR '96)*, June (1996) 196-202.

[9] C.-H. Kuo, Y.-L. Tsai, F.-C. Huang and M.-Y. Lee, Development of image servo tracking robot for the surgical space positioning system, *IEEE International Conference on Systems, Man and Cybernetics,* 5, Hague, Netherlands, Oct. (2004) 4462-4467.

[10] A. Bonarini, P. Aliverti and M. Lucioni, An omnidirectional vision sensor for fast tracking of mobile robot, *IEEE Trans. On Instrumentation and Measurement*, 49 (3) (2000) 509-512.

[11] X. Yang and A. Tayebi, Vision based trajectory tracking controller for a B21R mobile robot, *International Robots and Systems, 2006, IEEE/RSJ International Conference*, Beijing China, Oct. (2006) 3313-3318.

[12] A. Bais and R. Sablatnig, Landmark based global self-localization of mobile soccer robots, *Proceedings ACCV'06 of the 7th Asian Conference on Computer Vision*, II (2006) 842-851.

[13] K. Sabe, M. Fukuchi, J.-S. Gutmann, T. Ohashi, K. Kawamoto and T. Yoshigahara, Obstacle avoidance and path planning for humanoid robots using stereo vision, *ICRA 2004, International Conference on Robotic and Automation*,

1, New Orleans, USA (2004) 592-597.
[14] H. Chen and Z. Xu, 3D map building based on stereo vision, *Proceedings of the Networking, Sensing and Control, ICNSC'06,* Lauderdale, FL, USA (2006) 969-973.
[15] A. Elfes, Using occupancy grids for mobile robot perception and navigation, *Computer,* 22 (6) (1989) 46-57.
[16] S. Wang, X. Wang and H. Chen, A stereo video segmentation algorithm combining disparity map and frame difference, *Proceedings of 3rd International Conf. on Intelligent System and Knowledge Engineering*, Xiamen, China, Nov. (2008) 1122-1125.
[17] S.-J. Huang and J.-S. Lee, A stable self-organizing fuzzy controller for robotic motion control, *IEEE Transactions on Industrial Electronics*, 47 (2) (2000) 421-428.
[18] S.-J. Huang and W.-C. Lin, Adaptive fuzzy controller with sliding surface for vehicle suspension control, *IEEE Transactions on Fuzzy Systems*, 11 (4) (2003) 550-559.
[19] L. T. Wang and C. C. Chen, A combined optimization method for solving the inverse kinematics problem of mechanical manipulator, *IEEE Transactions On Robotics and Automation,* 7 (4) (1991).
[20] K. Kazerounian, On the numerical inverse kinematics of robotic manipulator, *AMSE J. of Mechanisms, Transmissions and Automation in Design,* 109 March (1987) 8-13.
[21] Texas Instruments Inc., *Applications using the TMS320C 6000 enhanced DMA reference guide*, October (2001).
[22] R. C. Gonzalez and R. E. Woods, *Digital image processing,* Addison-Wesley (1992).
[23] H.-T. Sheu, H.-Y. Chen and W.-C. Hu, Consistent symmetric axis method for robust detection of ellipses, *IEE Proceedings, Vision, Image and Signal Processing*, 144 (6) December (1997) 332-338.
[24] J.-S. Lee, C.-W. Seo and E.-S. Kim, Implementation of opto-digital stereo object tracking system, *Optics Communications*, 200 (2001) 73-85.
[25] A. J. Lipton, H. Fujiyoshi and R. S. Patil, Moving target classification and tracking from real-time video, *Proc. IEEE Workshop on Application of Computer Vision*, Princeton, NJ, USA Oct. (1998) 8-13.
[26] M. Sonka, V. Hlavac and R. Boyle, *Image processing analysis and machine vision*, United States of American, Thomson (2008).
[27] N. Otsu, A threshold selection method from gray-level histograms, *IEEE Trans. On Systems, Man and Cybernetics,* SMC-9, 1 (1979) 62-66.
[28] J-J. E. Slotine, *Applied nonlinear control*, Prentice Hall (1991).
[29] C. H. Edwards and S. K. Spurgeon, *Sliding mode control – theory and applications*, Taylor &Francis Ltd., London, Bristol (1998).
[30] G. C. Hwang and S. C. Lin, A stability approach to fuzzy control design for nonlinear systems, *Fuzzy Sets Systems*, 48 (1992) 269-278.

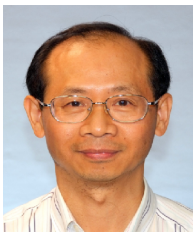

Shiuh-Jer Huang received the B.Sc. and M.Sc. from National Taiwan University, Taipei, Taiwan, and the Ph.D. from the University of California, Los Angeles, USA, in 1978, 1980 and 1986, respectively, all in Mechanical Engineering. In 1986, he joined the faculty of the Department of Mechanical Engineering, National Taiwan University of Science and Technology, Taipei, Taiwan, where he is currently a Professor. His research interests are precision mechatronics control, intelligent control system, robotic system control, vision servo motion control and advanced vehicle components development and applications.

Sheng Liu received the M.Sc. Degree from the Department of Mechanical Engineering, National Taiwan University of Science and Technology, Taipei, Taiwan, in 2011. Now he is working in Pegatron Corporation as a system integration engineer.

Chun-His Wu received the M.Sc. Degree from the Department of Mechanical Engineering, National Taiwan University of Science and Technology, Taipei, Taiwan, in 2011. Now he is working in Pegatron Corporation as a system integration engineer.